 CMES, vol.55, no.2, pp.171-190, 2010

An Investigation of Metal 3D Spheroidal Resonators Using a Body of Revolution Approach

A. Vukovic[1], P. Sewell[1] and T. M. Benson[1]

Abstract: A fast and accurate method is developed for the analysis of a class of metal three-dimensional resonators with rotational symmetry. The analysis is formulated using the Body of Revolution approach and the Method of Analytical Regularization. This development is motivated by the need for three-dimensional analytical solvers that could enable fast and accurate analysis of photonic resonant structures which support very high Q whispering gallery modes and which are computationally challenging for numerical simulations. The paper outlines the formulation of the method and demonstrates the stability and the source of computation errors of the method. As a practical illustration, the values obtained for the resonant frequencies of metal prolate and oblate resonators are compared with results from both numerical and exact analytic methods.

Keywords: Body of revolution, integral equation method, Method of Analytical Regularization, metal spheroids.

1 Introduction

Body of Revolution (BOR) approaches employ techniques for modeling a class of three dimensional geometries as equivalent two dimensional problems without introducing any physical approximation. The methodology is generally applicable to objects with rotational symmetry, i.e., those that can be obtained by rotating a generic arc around an axis of symmetry. In essence, the approach involves building into the integral or differential equations that describe the physical processes the fact that the geometry is a body of revolution so that it is no longer necessary to explicitly sample the fields in all three dimensions. In practice, the question is whether using these more complex equations over a lower dimension problem space is computationally preferable to using the original simpler equations over a larger problem space?

[1] George Green Institute for Electromagnetics Research, Faculty of Engineering, University of Nottingham, U.K.

To date, integral equation (IE) methods exploiting this equivalency have mainly been applied to electromagnetic scattering problems and for example, have been widely used in antenna and radar research [Andreasen, M.G, (1964), L. Marin (1974), Glisson W. (1978), Glisson W. and Willton D. R. (1980), T.K. Wu, (1989), Abdelmageed K. (2000)].

This paper focuses on IE methods that construct a modified free space Green's function which rather than give the fields radiated by a point source, give the fields radiated by a continuous ring of point sources with a prescribed angular dependence. However, it is noted that body of revolution objects have also been modeled using similar principles in conjunction with numerical methods such as the Method of Moments (MM), Finite Element (FE) and Finite Difference Time Domain (FDTD) methods, (Yuceer, M., Mautz, J.R., and Arvas, E. (2005), Morgan, M. and Mei, K., (1979), Farahat, N., Yu, W. and Mittra R. (2003)).

The key to obtaining a practical advantage from the BOR IE formulation is the identification of a computationally efficient description of the modified free space Green's function: naturally, it is expected that the behavior of this function is more complex than that of the simple point source Green's function. To proceed, it is first convenient to express the modified form of the free space Green's function as a Fourier series with respect to the azimuthal angle ϕ. Each term of this series is given by an integral over ϕ of the free space Green's function and a harmonic angular dependence of the fields, for example $e^{-jm\varphi}$, and this is referred to as the Modal Green's function (MGF). It is noted that in a BOR the MGF terms for different values of m are physically uncoupled by the rotational symmetry.

The kernel of an IE formulation of a BOR problem contains the MGF and as this function is highly oscillatory, the major demand upon computational time when solving for the fields is its evaluation for the purpose of numerical integration. Therefore, simpler and computationally faster forms of the MGF have been sought in the form of convergent series representations although, to date, these have mainly be applied to the study of antenna problems, limiting the investigations to slim or moderately thick bodies [Yu W. M., Fang D. G. and Cui T. J. (2008), Wang W. X. (1992), Werner D. H. (1999), Lim P., Li L.W. and Li E.P. (2002)]. Furthermore, series acceleration methods and asymptotic extraction have also been applied to the series expansion of the MGF with good success [Abdelmageed K. (2000)].

Unfortunately, computationally efficiency is further compromised by the presence of singular points of the kernel and more generally sharp peaks which are physically a consequence of evaluating fields in close proximity to source points. Therefore, it is also important to remove this behavior from the kernel and this can be achieved by identifying the local characteristics of the kernel and introducing yet another representation of the MGF which is rapid to evaluate in the vicinity of these peaks.

In this paper, the BOR integral equations are reduced to second-kind equations of the Fredholm type using the Method of Analytical Regularization (MAR) [Nosich A. (1999)]. This is achieved by using canonical shape extraction and by an appropriate choice of the expansion functions used to represent the fields on the surface of the geometry. This approach will be shown to substantially reduce the sharp peaks of the functions that need to be integrated numerically and thus yield a significantly more robust algorithm.

Canonical shape extraction is a physically based singularity extraction technique which exploits the fact that the numerical integrations that need to be evaluated become analytic for particular canonical geometries and are thus easy to evaluate in closed form. Therefore, rather than perform the numerical integrations directly on the integrand arising from the general BOR, they are actually performed on the difference between the integrands arising from the actual BOR and those from the canonical shape. As both the BOR and canonical shape integrands exhibit similar sharp peaks, this results in smoother and more robust numerical integrations. The general behavior of the MGF around the sharp peaks is discussed further below and the advantages of the regularization process in terms of the algorithm's accuracy and stability are illustrated. However, it shall also be shown below that even using canonical shape extraction, the numerical robustness is still affected by the choice of basis functions used to expand the field unknowns. In this paper the Galerkin method is used to discretize the integral equations and the results obtained with two different types of expansion functions are compared. As an example application, the method is used to model 3D spheroidal metal resonators and the results obtained compared with those obtained using an exact variational approach [Li L.W., Kang X.K. and Leong M.S. (2001)] and the unstructured mesh numerical Transmission Line Modeling (TLM) method [Sewell P., Benson T.M., Christopoulos C., Thomas D. W. P., Vukovic A. and Wykes J.G., (2005)].

The following section introduces the concept of the MAR, its application to the BOR method for the case of a metal body and the MGF function. Section 3 summarizes the main implementation details and sections 4 and 5 present the numerical results and the main conclusions of the paper, respectively.

2 Mathematical formulations

2.1 The MAR method

The Method of Analytical Regularization (MAR) transforms first kind integral equations to second kind integral equations of the Fredholm type with a smoother kernel [Nosich A. (1999)]. The general first-kind integral equation can be written

in operator notation as

$$\hat{C}X = Y \tag{1}$$

where X and Y represent unknown and given functions respectively. By splitting the operator $\hat{C}$ into two parts $\hat{C} = \hat{C}_1 + \hat{C}_2$, where the first operator has a known inverse $\hat{C}_1^{-1}$, the original equation can be re-expressed as the second kind integral equation

$$\left(\hat{I} + \hat{H}\right) X = B \tag{2}$$

where $\hat{H} = \hat{C}_1^{-1}\hat{C}_2, B = \hat{C}_1^{-1}Y$, and $\hat{I}$ is the identity operator.

Mathematically, eq.(2) is of the Fredholm type if the inverted operator $\hat{C}_1$ is singular and $\hat{C}_2$ regular. When the continuous integral equations are discretized with N basis terms, the truncated form of eq.(2) is given by

$$X^N + \hat{H}^N X^N = B \tag{3}$$

The significant attraction of eq.(2) is that there are theoretical guarantees available regarding its convergence as the order of discretization is increased: specifically as N increases the relative error is theoretically only bounded by machine precision. This is not the case with eq.(1).

Clearly, the key question when considering the MAR is the identification and extraction of the operator $\hat{C}_1$ which must be amenable to analytic inversion in a convenient manner. To date this has been done in three ways: a) by extracting the static part, b) by extracting the asymptotic high frequency part or c) by extracting the frequency dependent part corresponding to a canonical shape [Nosich A. (1999)]. The canonical shape can be a circle in two-dimensions or a sphere in three-dimensions as both of these geometric forms are amenable to exact solution using the separation of variables and thus it is straightforward to construct their inverses in terms of two or three dimensional harmonic series. Finally, the choice of expansion functions is also important as if these can be chosen to be the orthogonal eigenfunctions of $\hat{C}_1$ then the singular operator $\hat{C}_1$ is also diagonalised and the convergence of the scheme is further improved [Nosich A. (1999)].

2.2 MAR regularization of the Body of Revolution integral equations

Body of Revolution objects are obtained by rotating a so-called generic arc around an axis of symmetry. Fig. 1 shows a hollow metal object which is a body of revolution placed in a medium of dielectric constant ε_{r1} and below we present a formulation to enable its interior resonances to be identified. From here on it is

convenient to describe the geometry of the object using the parametric coordinates t and φ, where t defines the arc-length of the body and φ is the azimuthal angle, as shown in Fig.1.

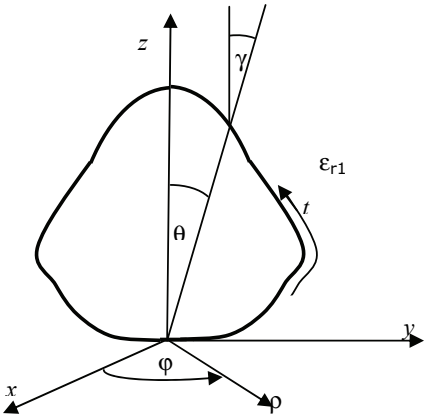

Figure 1: Geometry of the body of revolution. ρ, ϕ and z form a cylindrical coordinate system.

The boundary conditions on the metal surface require that the tangential electric fields vanish at the surface of the body. The scattered tangential electric fields can be expressed as, [Abdelmageed K. (2000)],

$$\vec{E}^s(\vec{r}) = -j\omega\vec{A}(\vec{r}) - \nabla\Phi(\vec{r}) \tag{4}$$

where $\vec{A}$ and Φ denote vector and scalar field potentials defined respectively by

$$\vec{A}(\vec{r}) = \frac{\mu_o}{4\pi}\int_S \vec{J}\left(\vec{r'}\right)\, G\left(\vec{r},\vec{r'}\right) dS', \tag{5}$$

$$\Phi(\vec{r}) = \frac{1}{4\pi\varepsilon}\int_S \nabla'\cdot\vec{J}\left(\vec{r'}\right)\, G\left(\vec{r},\vec{r'}\right) dS', \tag{6}$$

$\vec{J}$ is the electric surface current density vector that is to be found and $G\left(\vec{r},\vec{r'}\right)$ is the free space Green's function given by

$$G\left(\vec{r},\vec{r'}\right) = \frac{e^{-jkR}}{R} \tag{7}$$

$$R = \left|\vec{r}-\vec{r'}\right| = \left(\rho^2+\rho'^2-2\rho\rho'\cos\left(\phi-\phi'\right)+\left(z-z'\right)^2\right)^{1/2}$$

where the free space wavenumber $k = \frac{1}{\omega\sqrt{\varepsilon\mu_o}}$.
Substituting eqs.(5,6) into eq.(4) gives

$$\hat{n} \times \vec{E}(\vec{r}) = \left[\iint\limits_S \vec{J}\, GdS' + \frac{1}{k^2} \nabla \iint\limits_S \left(\nabla' \cdot \vec{J} \right) GdS' \right] = 0. \tag{8}$$

In order to generate second kind Fredholm equations, canonical shape extraction is performed by adding and subtracting the case of a perfect sphere from eq.(8). The tangential electric fields are thus given by

$$\begin{aligned} \hat{n} \times \vec{E}(\vec{r}) = & \left[\left\{ \iint\limits_S \vec{J}\, GdS' + \frac{1}{k^2} \nabla \iint\limits_S \left(\nabla' \cdot \vec{J} \right) GdS' \right\} \right. \\ & \left. - \left\{ \iint\limits_{S_o} \vec{J}\, G_o dS'_o + \frac{1}{k^2} \nabla \iint\limits_{S_o} \left(\nabla' \cdot \vec{J} \right) G_o dS' \right\} \right] \\ & + \left[\iint\limits_{S_o} \vec{J}\, \tilde{G}_o dS'_o + \frac{1}{k^2} \nabla \iint\limits_{S_o} \left(\nabla' \cdot \vec{J} \right) \tilde{G}_o dS'_o \right] = 0. \end{aligned} \tag{9}$$

The surface S_o denotes the surface of a perfect sphere of radius a. Both G_o and $\tilde{G}_o$ represent the Green's function for source points on this sphere and the tilde is being used here to emphasize that it is being expressed in different forms. Overall, the new terms in eq.(9) are introducing the field that would be produced if the surface current on the BOR were on the surface of the sphere. Therefore the net effect of the first two lines of eq.(9), which is the operator $\hat{C}_2$ above and which will be evaluated by numerical integration, will be small if the BOR were a perturbation on a sphere and even for large deviations, the problematic sharp peaks arising in the integrations tend to cancel. This leaves the second line of eq.(9) which is the operator $\hat{C}_1$ above and can be analytically inverted.

G_o is expressed in the form of eq.(7) and $\tilde{G}_o$ is the well known spherical harmonic representation of the free space Greens function [Morse and Feshbach, (1953)], i.e.,

$$G_o\left(\vec{r}, \vec{r'}\right) = \frac{e^{-jkR_o}}{R_o} \tag{10}$$

$$R_o = \left| \vec{r}_o - \vec{r'}_o \right| = \left(\rho_o^2 + a^2 - 2\rho_o a \cos\left(\phi_o - \phi'_o\right) + \left(z_o - z'_o\right)^2 \right)^{1/2}$$

and

$$\tilde{G}_o\left(\vec{r},\vec{r'}\right) = -jk\sum_{n=0}^{\infty}(2n+1)\sum_{m=0}^{n}\eta_m\frac{(n-m)!}{(n+m)!}\cos\left(m\left(\phi_o-\phi_o'\right)\right)$$
$$P_n^m(\cos\theta_o)P_n^m\left(\cos\theta_o'\right)\begin{cases} j_n(kr_o')\,h_n(kr_o), & r_o > r_o' \\ j_n(kr_o)\,h_n(kr_o'), & r_o < r_o' \end{cases} \quad (11)$$

where $P_n^m(\cos\theta)$ denote associated Legendre polynomials whose indices n and m represent the radial and azimuthal orders respectively. j_n and h_n are the spherical Bessel functions of the first and the third kind, and η_m=1 for m=0 and η_m=2 for $m \neq 0$.

In the next stage of the MAR approach, eq.(9) is discretisized using the Galerkin procedure and the choice of expansion functions for the surface current density should ideally be chosen to permit full diagonalisation of the operator $\hat{C}_1$, i.e. the third line of eq.(9), and hence reduction to the form of eq.(2).

The expansion of the electric surface currents in previous BOR formulations employed frequency independent basis terms: specifically the electric currents were expanded by pulse functions with respect to the t-direction and a Fourier series with respect to the φ-direction [Glisson W. (1978), Glisson W. and Willton D. R. (1980)], or with the high frequency asymptotic basis terms $J_n^m(\vec{r'}) = \sum_m [A_n^m t' + B_n^m \varphi']e^{-jm\varphi'}$ [Abdelmageed K. (2000)]. However, neither of these choices diagonalises the operator $\hat{C}_1$. In this paper, the electric surface currents are expanded in terms of frequency dependent spherical waves defined on the surface of the perfect sphere with a view to accomplishing this diagonalisation. The paper investigates two particular expansion forms: the scalar high-frequency expansion which is defined as [Vukovic, A., Sewell, P., and Benson T. M. (2009)],

$$J_n^m\left(\vec{r'}\right) = \sum_m\sum_n\left[A_n^m P_n^m\left(\cos\theta_o'\right)\vec{t'} + B_n^m P_n^m\left(\cos\theta_o'\right)\hat{\phi}'\right]e^{-jm\phi'} = J_t^{n,m}\hat{t'} + J_\phi^{n,m}\hat{\phi}', \quad (12)$$

and the full vector expansion form that uses a vector harmonic spherical wave expansion, [Li L.W., Kang X.K., Leong M.S. (2001)], i.e.,

$$J_n^m\left(\vec{r'}\right) = \sum_m\sum_n\left[A_n^m\left((J_t^{n,m})^{TE}\vec{t'} + \left(J_\phi^{n,m}\right)^{TE}\hat{\phi}'\right) + B_n^m\left((J_t^{n,m})^{TM}\vec{t'} + \left(J_\phi^{n,m}\right)^{TM}\hat{\phi}'\right)\right], \quad (13)$$

where

$$(J_t^{n,m})^{TE} = -\frac{\partial P_n^m(\cos\theta_o')}{\partial t'}\cos\left(m\phi'\right),$$

$$\left(J_\phi^{n,m}\right)^{TE} = -\frac{jm}{\sin\theta_o'}P_n^m\left(\cos\theta_o'\right)\sin\left(m\phi'\right),$$

$$(J_t^{n,m})^{TM} = \frac{jm}{\sin\theta_o'}P_n^m\left(\cos\theta_o'\right)\sin\left(m\phi'\right),$$

$$\left(J_\phi^{n,m}\right)^{TM} = \frac{\partial P_n^m(\cos\theta_o')}{\partial t'}\cos\left(m\phi'\right).$$

In both eq.(12) and eq.(13) A_n^m and B_n^m are unknown coefficients to be found.

Although the scalar form, eq.(12), does not diagonalise $\hat{C}_1$ it merits investigation as it is notably simpler than the vector basis terms which do diagonalise $\hat{C}_1$. In both cases, eq.(9) is solved for the unknown coefficients A_n^m and B_n^m for a prescribed azimuthal order m. Application of Galerkin's method, i.e., performing term-by-term testing and integration for all the entire domain expansion functions n=0,1,2,...,N, results in a final matrix problem of order $2N\times 2N$ which exhibits a zero determinant for those frequencies at which a resonance of the BOR occurs. This process can then be repeated independently for each value of azimuthal order m of interest. More details of the numerical integrations are described in section 3 of this paper.

2.3 The Modal Green's Function

The rotational symmetry of the resonator permits expansion of the Green's function in terms of spherical harmonics using the so-called Modal Green's function (MGF). For clarity this is shown in the context of the first term of eq.(9) with the expansion given in eq.(12),

$$\iint_S \vec{J}\,G dS' = \int_0^{\pi} r' d\theta' \int_0^{2\pi} d\varphi' \left[\sum_n \left[A_n^m P_n^m\left(\cos\theta_o'\right)\vec{t}' + B_n^m P_n^m\left(\cos\theta_o'\right)\hat{\phi}'\right]\right]\frac{e^{-jkR}}{R}e^{-jm\varphi'} \quad (14)$$

Eq.(14) shows that the azimuthal integration can be incorporated into the Modal Green's function as:

$$G^m\left(\vec{r},\vec{r'}\right) = \frac{1}{\pi}\int_0^{2\pi}\frac{e^{-jk_iR}}{R}e^{-jm(\phi-\phi')}d\left(\phi-\phi'\right). \quad (15)$$

This illustrates the discussion of the introductory paragraph: eq.(15) is now more complex than the simple free space Green's function, but the expansion functions representing surface currents on the BOR effectively need only span one dimension (i.e. t in Fig.1).

As stated above, the MGF function is highly oscillatory and its efficient computation is generally only available using the series expansion [Abdelmageed K. (2000)]

$$G^m\left(\vec{r},\vec{r'}\right) = \frac{e^{-jk_iR_b}}{R_b}\delta_{m,0} - jk\sum_{q=1}^{\infty} A_q^m h_q^{(2)}\left(kR_b\right)\left(\frac{k^2\rho\rho'}{kR_b}\right)^q, \tag{16}$$

where $R_b = \left(\rho^2 + \rho'^2 + (z-z')^2\right)^{1/2}$, $h_q^{(2)}$ represents the spherical Hankel function of the 3^{rd} kind and the coefficients A_q^m are evaluated using recurrence formulae [Abdelmageed K. (2000)].

Substituting the finite power series form of the spherical Hankel function in eq.(16) [Abdelmageed K. (2000)]

$$h_q^{(2)}(x) = j^{(q+1)}\frac{e^{-jx}}{x}\sum_{i=0}^{q}\frac{(q+i)!}{i!\,(q-i)!}\frac{1}{(j2x)^i} \tag{17}$$

results in the following form of the MGF which is most suitable for rapid computation.

$$G^m\left(\vec{r},\vec{r'}\right) = \frac{e^{-jk_iR_b}}{R_b}\left[\delta_{m,0} + \sum_{q=1}^{\infty}\sum_{i=0}^{q} B_{q,i}^m\frac{\left(k^2\rho\rho'\right)^q}{\left(kR_b\right)^{q+i}}\right]. \tag{18}$$

The coefficients $B_{q,i}^m$ are again found using recurrence and need to be obtained only once as they are independent of both frequency and the coordinates of the source and observation points formulae [Abdelmageed K. (2000)].

Unfortunately, the presence of the free space Green's function singularity at $r = r'$ undermines the convergence of (eq.(18)) in the vicinity of $R_b = 0$ and therefore [Abdelmageed K. (2000)] extracted this singularity from the MGF by re-expressing eq.(15) as

$$G^m\left(\vec{r},\vec{r'}\right) = \frac{1}{\pi}\int_0^{\pi}\left(\frac{e^{-jk_iR}}{R}e^{-jm\beta} - \frac{1}{R}\right)d\beta + \frac{1}{\pi}\int_0^{\pi}\frac{1}{R}d\beta, \tag{19}$$

whereby the first term is now a smooth function and the second term can be evaluated in closed form as a complete elliptic integral of the first kind: the remaining

logarithmic singularity of the latter being extracted analytically along the generic arc [Glisson W. (1978)].

At this point it is important to note that the only true singularity of the MGF occurs at R_b=0, and as $R_b = \left(\rho^2 + \rho'^2 + (z-z')^2\right)^{1/2}$, and as we see that this can only occur if $z = z'$ and $\rho = \rho'$ generally only corresponds to both the source and observation points being located at the exact top and bottom of BOR. However, even for general locations on the surface of the BOR, the MGF still exhibits a sharp peak as t approaches t' and although not an exact singularity, numerically these are equally problematic and must be dealt with carefully.

3 Numerical details

This section outlines the main details for the numerical implementation of the BORMAR method. For background details the reader is referred to [Glisson W. (1978) and Glisson W., Willton D.R., (1980)].

The parametric coordinates t and ϕ, introduced in Fig.1, are related to the Cartesian coordinates through:

$$\hat{t} = \hat{z}\cos\gamma + \hat{x}\sin\gamma\cos\phi + \hat{y}\sin\gamma\sin\phi \tag{20}$$

$$\hat{\phi} = -\hat{x}\sin\phi + \hat{y}\cos\phi \tag{21}$$

In the parametric system t and ϕ, it is straightforward calculus to show that the components of the gradient and divergence for an arbitrary vector function Ψ are:

$$\begin{aligned}
\hat{t}\cdot\nabla\Psi &= \frac{\partial}{\partial t}\Psi, \\
\hat{\phi}\cdot\nabla\Psi &= \frac{1}{\rho}\frac{\partial}{\partial\phi}\Psi, \\
\nabla\cdot\hat{t}\Psi_t &= \frac{1}{\rho}\frac{\partial}{\partial t}\rho\Psi_t, \\
\nabla\cdot\hat{\phi}\Psi_\phi &= \frac{1}{\rho}\frac{\partial}{\partial\phi}\rho\Psi_\phi
\end{aligned} \tag{22}$$

where Ψ_t and Ψ_ϕ respectively denote the t and ϕ components of the vector Ψ.

Using the identities in eqs.(20-22) and taking into account that the azimuthal part of the surface integral $\int_S' dS' = \int_0^{2\pi} d\phi' \int_0^{t_{\max}} \rho' dt'$ has become absorbed within the MGF,

G^m, the tangential components of eq.(8) become:

$$\vec{t}\cdot\left(\iint_S \vec{J}GdS' + \frac{1}{k^2}\nabla\iint_S\left(\nabla\cdot\vec{J}\right)GdS'\right) =$$
$$\left(\int_0^{t_{\max}}\rho' dt'\left(\cos\gamma\cos\gamma' G^m + \sin\gamma\sin\gamma'\left(\frac{G^{m-1}+G^{m+1}}{2}\right)\right)J'^m_t + \right.$$
$$\left.\sin\gamma\left(\frac{G^{m-1}-G^{m+1}}{2j}\right)J'^m_\phi\right) + \qquad (23)$$
$$+\frac{1}{k^2}\frac{\partial}{\partial t}\left(\int_0^{t_{\max}}\rho' dt' G^m\left(\frac{1}{\rho'}\frac{\partial}{\partial t'}\rho' J'^m_t + \frac{jm}{\rho'}J'^m_\phi\right)\right)$$

$$\hat{\phi}\cdot\left(\iint_S \vec{J}GdS' + \frac{1}{k^2}\nabla\iint_S\left(\nabla\cdot\vec{J}\right)GdS'\right) =$$
$$\left(\int_0^{t_{\max}}\rho' dt'\left(-\sin\gamma'\right)\left(\frac{G^{m-1}-G^{m+1}}{2j}\right)J'^m_t + \left(\frac{G^{m-1}+G^{m+1}}{2}\right)J'^m_\phi\right) \qquad (24)$$
$$+\frac{1}{k^2}\frac{1}{\rho}\frac{\partial}{\partial\phi}\left(\int_0^{t_{\max}}\rho' dt' G^m\left(\frac{1}{\rho'}\frac{\partial}{\partial t'}\rho' J'^m_t + \frac{jm}{\rho'}J'^m_\phi\right)\right)$$

Eqs.(23,24) represent the original BOR formulation without using the MAR canonical shape extraction (i.e. eq.(8)) [Glisson W. (1978), Glisson W., Willton D.R., (1980), Abdelmageed K. (2000)].

The formulation of this work based upon eq.(9) and its first term is also directly given by eqs.(23-24). Similarly, the second and the third terms of eq.(9) have the same expanded forms as eqs.(23,24) but are defined for the sphere of radius $r = a$ and use the Green's function defined for the sphere G_o or $\tilde{G}_o$ respectively.

The Galerkin discretisation of the third term of eq.(9) that contains the spherical harmonic expansion of the Green's function (eq.(11)) can be evaluated analytically whilst the first and the second term integrations are performed numerically. The radius of the sphere, a, is chosen such that the generic arcs of the sphere and the BOR have the same length. Experimentation has shown that this provides a good extraction of the source point peaks.

As the singular point $R_b = 0$ of the MGF occurs when t=0 and t=t_{max}, it is also helpful to undertake the change of variable $t = \frac{1}{2}(w+1)\ t_{\max}$ where -1<w<1 and subsequently define $w = -\cos(\nu)$ with $0 < \nu < \pi$.

Overall, this change of variables transforms the numerical integrations as

$$\int_{o}^{t_{\max}} \rho dt = \int_{0}^{\pi} \rho \frac{\partial t}{\partial \nu} d\nu = \int_{0}^{\pi} \rho \sin \nu \frac{t_{\max}}{2} d\nu$$

where the term $\sin \nu$ has zeros where the MGF has a true singularity.

4 Results

This section presents numerical results demonstrating the accuracy and stability of the algorithm. First, the singular behavior of the MGF integral is analyzed and the effectiveness of the singularity extraction within the BOR-MAR method is demonstrated. In order to verify the accuracy of the method, the self-consistent convergence of the relative error of the method is considered and then to verify the absolute accuracy, results obtained for the resonant frequencies of a range of spheroids are compared to those obtained using an exact variational method [Li L.W., Kang X.K., Leong M.S. (2001)] and numerical simulations based upon an unstructured mesh geometry description[Sewell P., Benson T.M., Christopoulos C., Thomas D. W. P., Vukovic A. and Wykes J.G., (2005)]. All the BOR-MAR computations are performed in double precision on a standard desktop PC.

Spheroids are obtained by rotating the generic arc of an ellipse with major and minor radii defined as r_x=1 μm and $r_z = r_x \alpha$ about an axis and prolate and oblate spheroids correspond to the ranges 0<$\alpha < 1$ and α>1 respectively. These structures are chosen for validation purposes due to the availability of benchmark quality results.

Fig.2 shows the behavior of the MGF function along the generic arc over which the numerical integrations must be performed for the case of the oblate spheroid defined by α=0.9. The values are obtained using the series expansion given by eq.(18) and for comparison by numerically evaluating the MGF integral of eq.(15). The generic arc contour is divided into 100 uniform segments, Δt. As discussed at the end of section 2, a sharp peak occurs when R_b is minimal which in this illustration occurs at $t = t'$=40Δt. The series expansion of the MGF is shown when the series of eq.(18) is truncated to 10, 50 and 85 terms. As a reference, the MGF is also evaluated directly from eq.(15) numerically using 10^5 integration points which is very slow but accurate, except when close to the centre of the peak. The MGF function is shown for azimuthal orders m=0 and m=5.

Fig.2 shows that the direct integral evaluation of the MGF clearly exhibits quasi-singular behavior at $t = t'$ whilst the truncated series representations notably smooth out this peak. This confirms that in the vicinity of the peak, the series convergence

of the MGF function is unacceptably slow and does not adequately capture the quasi-singular behavior of the MGF integral. It is noted that in practice the number of terms that can be used in the series is limited by loss of precision caused by adding large values of opposite signs. This lack of accuracy is more pronounced for higher azimuthal orders as shown in Fig.2b and overall these observations provide the motivation for performing the MAR: removal of these sharp peaks from the numerical integrations.

To demonstrate the effect of canonical shape extraction Fig.3 plots the difference between the MGF integrands arising from the actual BOR and those of the perfect sphere. The BOR body is taken to be oblate spheroid with α=0.9 and the sphere of radius a is chosen such that both BOR body and the sphere have same lengths of generic arcs (a=0.950658). The difference in integrands is evaluated for the azimuthal order m=5 and is plotted for both integral and series representation of the MGF functions. It can be seen that in both cases peaks at quasi-singular points are cancelled resulting in a much smoother curve.

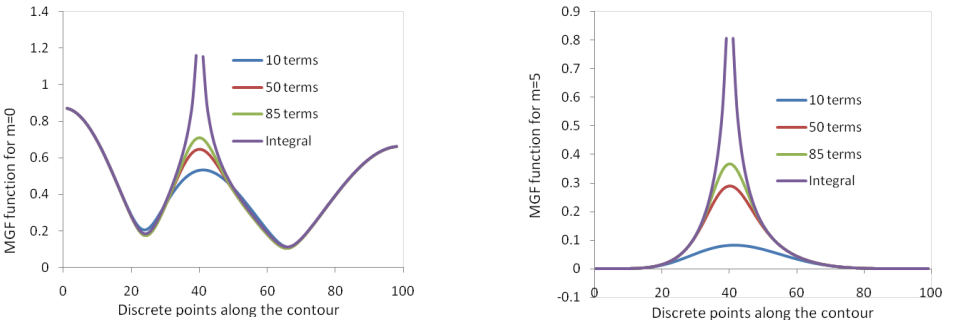

a) b)

Figure 2: Quasi-singular behavior of the MGF along the contour for a) m=0 and b) m=5 using 10, 50 and 85 terms in the series expansion eq.(18) and direct numerical integration of the MGF integral, eq.(14) using 10^5 points.

To demonstrate the consequences of the poor convergence of the MGF series in the vicinity of the peaks on a practical simulation, the TM02 mode resonant frequency of an oblate spheroid with α=0.9 is determined using the BOR formulation.

Fig.4 shows the relative error in this resonant frequency, f_r, with respect to the number of Legendre polynomial basis terms, N used to expand the surface currents in the manner of eq.(12). All numerical integrations sample at 100 points along the BOR contour. The relative error is calculated as $\left(f_r^{(N)} - f_r^{(N-1)}\right)/f_r^{(N)}$, which

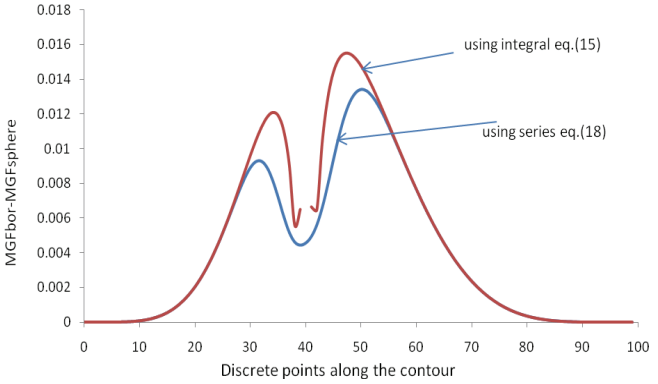

Figure 3: Integrand MGF_{BOR}-MGF_{sphere} for m=5. BOR body is taken to be oblate spheroid with α=0.9 and sphere of radius a=0.950658.

gives a measure of self-consistent convergence of the method in the presence of matrix truncation.

Three curves are given in Fig.4: (a) Using the standard BOR implementation with the singularity extracted kernel of [Abdelmageed K. (2000)], (eq.(19)), (b) using BOR-MAR with the singularity-extracted kernel of [Abdelmageed K. (2000)], i.e. eq.(19) and (c) using the BOR-MAR with the smooth kernel of eq.(18). It is immediately apparent that the standard BOR implementation does not converge and this is a direct consequence of the inaccuracy presented in Fig.2. However, it is well known that the relative error of the 2^{nd} kind equations of the Fredholm type produced by the MAR theoretically decreases as the order of the matrix increases and Fig.4 shows that in both BOR-MAR cases, the singularity-extracted and smooth kernel, the relative error decreases logarithmically. Moreover, the results obtained using the shape extraction with smooth kernel (eq.(18)) method are slightly lower than those using the singularity-extracted kernel. As an aside, it is commented that the alternate term oscillation of the relative error is explained by the two-term recurrence relationship satisfied by the derivatives of the Associated Legendre Polynomials [Abramowitz, M., Stegun, I. A. (1965)].

Fig.5 compares results for the TM02 resonant frequency of the BOR-MAR method obtained using the MGF function given in eq.(18) and eq.(19) for a range of spheroids, defined by the parameter α. All results were obtained with 10 Legendre polynomials as current basis functions (eq.(9)), 50 terms in the series MGF expansion, eq.(14), and 100 integration points along the contour. The two sets of results obtained are virtually indistinguishable.

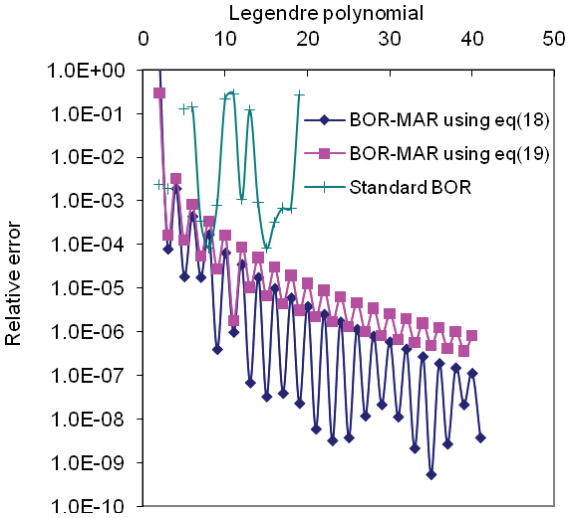

Figure 4: Relative error of the solution with respect to number of Legendre polynomials for the standard BOR, BOR-MAR method using the MGF function given in eq.(18) and BOR-MAR using the MGF function given in eq.(19).

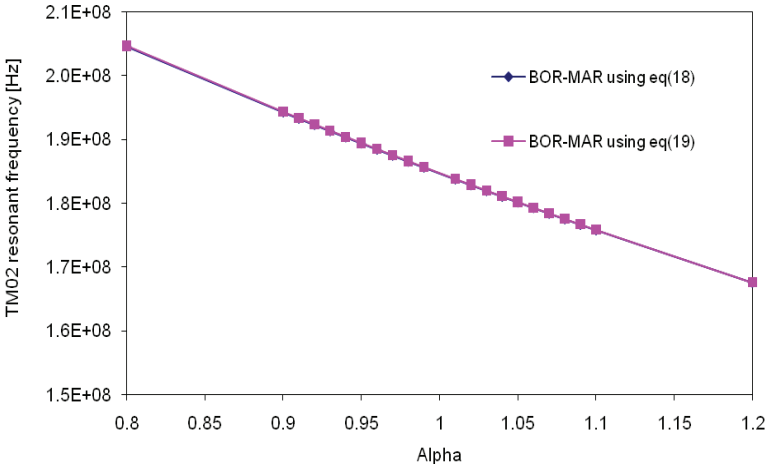

Figure 5: TM02 resonant frequency for a range of oblate and prolate spheroids with smooth and singular kernels.

Fig.6 compares the relative error of the resonant TM02 frequency as a function of the number of terms, n, used in the spherical harmonic representation of the free space Green's function, eq.(11). Clearly sufficient terms must be used to (a) capture the inherent order of the resonant fields being sought and also (b) to capture the deviation of the BOR structure from a perfect sphere. Fig 6. shows that for different oblate spheroids defined with α=0.8, 0.9 and 0.98 a sharp initial drop is followed by a slower improvement in accuracy and these two features are attributable to points (a) and (b) above. These results were obtained using canonical shape extraction MAR, 10 Legendre polynomials, eq.(12), 50 terms in eq.(18), and 100 sample points for the numerical integrations.

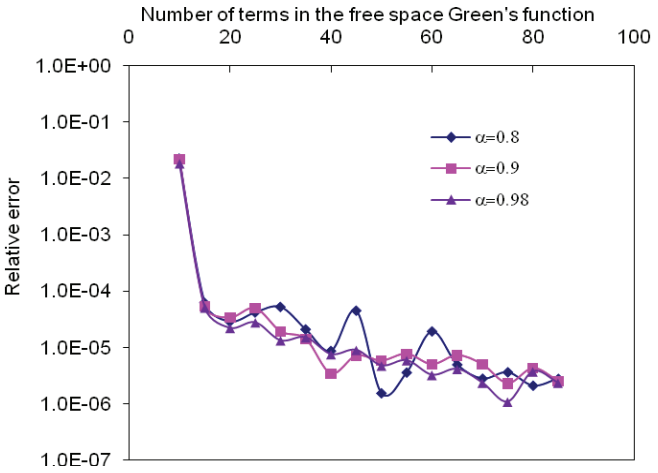

Figure 6: Relative error as a function of the number of terms in the free space Green's function for α=0.8,0.9 and 0.98.

The impact of the number of sample points used in the numerical integrations on the relative error is shown in Fig.7. Results are obtained using 10 Legendre polynomials, 50 terms in eq.(18), 50 terms in the spherical harmonic Green's function eq.(11) and for different oblate spheroids defined with α=0.8, 0.9 and 0.98. It can be seen that for accuracy greater than 10^{-5} a minimum of 100 integration points is needed. However, this is a relatively low value which is good for computational efficiency and demonstrates the success of the MAR at removing the sharp peaks from the integrands of the numerical integrations.

In order to provide independent validation of the accuracy, Fig.8(a,b) compares the results obtained using BOR-MAR approach against those obtained for a range of oblate and prolate spheroids with 0.8<α<1.2 using the variational approach [Li

L.W., Kang X.K., Leong M.S. (2001)] and the numerical TLM method based on unstructured meshes [Sewell P., Benson T.M., Christopoulos C., Thomas D. W. P., Vukovic A., Wykes J.G., (2005)]. The simulation parameters are obtained for 50 terms in eq.(18), 50 terms in eq.(11), 30 current basis terms and 100 integration points. Fig.8a) first shows the results obtained using the scalar basis functions for the surface currents given in eq.(12) and shows that, except for the case of very small sphere deformations $\alpha \sim 1$, the BOR-MAR results deviate unacceptably from both the variational and TLM results. This indicates that the scalar expansion, eq.(12) does not adequately capture the true surface current distributions with this number of expansion terms. The reason for this is that these basis functions do not diagonalise the operator $\hat{C}_1$ as explained above and this slows convergence with respect to the number of basis terms: specifically, the derivatives of the basis functions that are performed in eq.(23) and eq.(24) cause a wide cross-coupling of the basis terms. In contrast, Fig.8b) shows that BOR-MAR results obtained using the full vector expansion of the surface currents, eq.(13), agree very well with the numerical TLM results, which is consistent with the diagonalisation of $\hat{C}_1$ and the more compact cross-coupling of the basis terms due to differentiation. It is noted here that the variational results are obtained in the form of a series and for the larger and smaller values of α are expected to be less accurate due to the limited number of coefficients available in the literature. For convenience, all results are also given in Table 1.

An individual BOR-MAR result takes only a few minutes to calculate, indicating the computational efficiency of the method. This can be compared with the TLM results which are evaluated as an numerical eigenvalue problem in the frequency domain and require substantially more time per point. Depending upon the mesh density demanded by the accuracy and the spatial order of the mode being sought, the run times typically require 30 minutes using 4 parallel CPUs on an EV6 Alpha (1250MHz) SMP cluster.

5 Conclusions

In this paper the original Body of Revolution approach is reformulated as 2^{nd} kind Fredholm equations using Method of Analytical Regularisation and applied to metal spheroidal resonators. A number of key practical issues have been explored that strongly influence both the accuracy and the run time efficiency of the approach. It has been shown that the regularization process is essential in order to obtain convergence of the discretized problem and that using canonical shape extraction is superior to simple extraction of the singularity of the kernel. Good convergence has been shown with respect to both number of current expansion functions used as well as the number of sample points used to evaluate the nu-

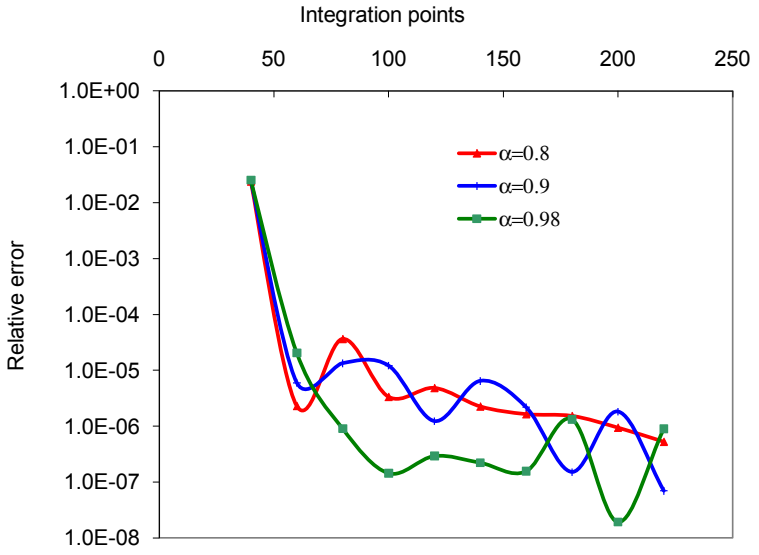

Figure 7: Relative error as a function of the number of integration points for α=0.8,0.9 and 0.98.

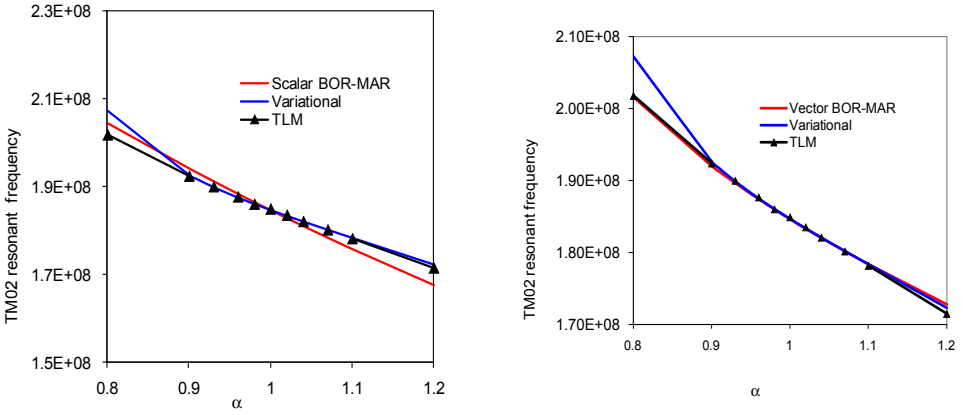

(a) (b)

Figure 8: Comparison of resonant frequencies for the oblate and prolate spheroids obtained using variational method, numerical TLM method and BOR-MAR method with a) the scalar expansion of the surface currents and b) the vector expansion for the surface currents

Table 1: Comparison of TM02 resonant frequency for spheroids with the major and minor axis r_x=1μm and $r_z = \alpha r_x$, obtained using Variational, TLM and BOR method with the scalar and vector expansion function.

	Frequency [MHz]			
Alpha	**Variational method**	**TLM**	**Vector BOR**	**Scalar BOR**
0.8	207.305	201.822	201.6530	204.596
0.9	192.673	192.422	192.0390	194.249
0.93	189.929	190.019	189.6860	191.308
0.96	187.542	187.710	187.461	188.412
0.98	186.085	186.052	186.045	186.524
1.	184.713	184.947	184.6790	184.672
1.02	183.383	183.549	183.344	182.830
1.04	182.101	182.113	182.058	181.024
1.07	180.228	180.190	180.184	178.371
1.1	178.391	178.196	178.403	175.773
1.2	172.330	171.518	172.812	167.529

merical integrations. Results for the resonant frequencies of oblate and prolate metal spheroids have been compared to those obtained using an exact variational approach and the numerical TLM method and demonstrate a good independent validation of the accuracy.

References:

Abramowitz, M., Stegun, I.A. (1965): *Handbook of Mathematical Functions*, Dover, New York.

Andreasen, M.G. (1964): Scattering from Bodies of Revolution, *IEEE Trans AP*, pp.303-310.

Abdelmageed K. (2000): Efficient evaluation of modal Green's functions arising in EM scattering by bodies of revolution, *Progress in Elecromagnetics Research*, PIER 27, pp.337-357.

Farahat, N., Yu, W., Mittra R. (2003): A Fast Near-to-Far-Field Transformation in Body of Revolution Finite-Difference Time-Domain Method, vol.51, no.9, pp:2534-2540.

Glisson W. (1978): *On the development of numerical techniques for treating arbitrary-shaped surfaces*, PhD thesis, Univ. Mississipi.

Glisson W., Willton D.R. (1980): Simple and efficient numerical methods for

problems of electromagnetic radiation and scattering from surfaces, *IEEE Trans. Antennas Propagat.*, vol.28, pp.593-603.

Li L.W., Kang X.K., Leong M.S. (2001): *Spheroidal Wave Functions in Electromagnetic Theory*, Wiley.

Lim P., Li L.W., Li E.P. (2002): Fast full-wave analysis of a cylindrical antenna using a single integral with an exact kernel, *IEEE Antennas and wireless Propagation Letters*, vol.1, pp. 43-45.

Marin L. (1975): Natural-Mode Representation of Transient Scattering from Rotationally Symmetric Bodies, *IEEE Trans. AP*, vol.22, no.2, pp266-274.

Morgan, M.; Mei, K. (1979): Finite-element computation of scattering by inhomogeneous penetrable bodies of revolution, *IEEE Trans AP*, vol. no.2, pp.202-214.

Morse; Feshbach (1953): *Methods of Theoretical Physics*, Part II, pp. 1466, McGrow-Hill.

Nosich A. (1999): The Method of Analytical Regularisation in wave-scattering and eigenvalue problems: Foundations and review of solutions, *IEEE Antennas and Propagation Magazine*, vol. 41, pp.34-49.

Sewell P., Benson T.M., Christopoulos C., Thomas D. W. P., Vukovic A., Wykes J.G. (2005): Transmission-line modeling (TLM) based upon unstructured tetrahedral meshes, *IEEE Transactions on Microwave Theory and Techniques*, vol. 53, pp.1919-1928.

Vukovic, A., Sewell, P., Benson T.M. (2009): Modeling 3D Spheroidal Resonators Using a Body of Revolution Approach, *Proc. of the 7^{th} UK Conference on Boundary Integral Methods*, UKBIM7, pp.25-28.

Wang W.X. (1992): The exact kernel for cylindrical antenna, *IEEE Trans. On Antennas and Propagation*, vol.39, no.4, pp.434-435.

Werner D.H. (1999): On a new cylindrical harmonic representation for spherical waves, *IEEE Trans on Antennas and Propagation*, vol.47, pp. 97-100.

Wu, T.K. (1989): Radar Cross Section of Arbitrary Shaped Bodies of Revolution, *Proc of IEEE*, vol.77, no.5, pp.735-740.

Yu W.M., Fang D.G., Cui T.J. (2008): Closed form modal Green's Functions for accelerated computation of bodies of revolution, *IEEE trans on Antennas and Propagat*., vol.56, pp.3452-3461.

Yuceer, M.; Mautz, J.R.; Arvas, E. (2005): Method of moments solution for the radar cross section of a chiral body of revolution, *IEEE Trans. AP*, vol.53, no.3, pp.1163-1167.